J Mater Sci (2008) 43:5930–5941
DOI 10.1007/s10853-008-2860-2

Droplet cooling in atomization sprays

Arvind Prasad · Hani Henein

Received: 17 April 2008 / Accepted: 3 July 2008 / Published online: 27 July 2008

Abstract Transport between droplets/particles and a gas phase plays an important role in numerous material processing operations. These include rapid solidification operations such as gas atomization and spray forming, as well as chemical systems such as flash furnaces. Chemical reaction rates and solidification are dependent on the rate of gas-particle or gas-droplet transport mechanisms. These gas-based processes are difficult to analyze due to their complexity which include particle and droplet distribution and the flow in a gas field having variations in temperature and velocity both in the jet cross-section and in the axial distance away from the jet source. Thus to study and properly identify the important variables in transport, these gas and droplet variations must be eliminated or controlled. This is done in this work using models based on a single fluid atomization system. Using a heat transport model (referred to as thermal model) validated using single fluid atomization of molten droplets and a microsegregation model, the effect of process variables on heat losses from droplets was examined. In this work, the effect of type of gas, droplet size, gas temperature, gas-droplet relative velocity on the heat transport from AA6061 droplets was examined. It is shown that for a given gas type, the most critical process variable is the gas temperature particularly as affected by two-way thermal coupling and the droplet size. The results are generalized and applied to explain the difference in droplet cooling rate from different atomization processes.

A. Prasad · H. Henein (✉)
Department of Chemical and Materials Engineering,
University of Alberta, Edmonton, Alberta, Canada T6G 2G6
e-mail: Hani.henein@ualberta.ca

List of symbols

A	Surface area of the droplet
Cp	Heat capacity of the droplet
Cp_{m}	Integral heat capacity
f_{s}	Fraction solid
Fo^*	Modified Fourier number for droplet-gas thermal transport
h_{total}	Total heat transfer coefficient
h_{conv}	Convective heat transfer coefficient
H	Droplet enthalpy
k_{s}	Gas thermal conductivity
ΔLatent	Solidification enthalpy
m and $(m+1)$	Indices for the numerical calculation
Nu	Droplet Nusselt number
Pr	Prandltl number
Re	Droplet Reynolds number
t	Time
t^*	Reference time
t_{f}	Solidification time
T_{liq}	Liquidus temperature of AA6061
T_{m}	Droplet temperature during solidification
T_{nuc}	Nucleation temperature for simulation
T_{sol}	Solidus temperature of AA6061
Tu	User-defined primary undercooled temperature
T_{∞}	Gas temperature in the free stream
V	Volume of the droplet
ρ	Droplet density
μ_{bulk}	Gas viscosities at the temperature of the free flow gas
μ_{surf}	Gas viscosities at the temperature of the droplet
θ	Dimensionless temperature
τ	Dimensionless time

Introduction

In materials processing, droplets are often used to process a wide range of liquids and slurries. The small size of the droplet enables high reaction rates or high solidification rates in many systems. To capitalize on these high rates of transport processes, sprays are developed to maximize throughput. The design of these sprays, however, does not account for the transport steps and rate limiting mechanisms at the droplet surface. Rather, spray design focuses on maximizing the break-up of a stream or slurry into small size droplets or controlling the spread of the spray. Spray systems in industrial use typically generate droplets of wide size distribution leading to a wide range of reaction or solidification times for droplets in the spray. This occurs because processing with a spray involves a number of coupled phenomena such as stream break-up and droplet-gas heat, momentum and mass transport, resulting in a droplet size distribution, spray geometry and particles which vary the extent of reaction or microstructure.

In gas sprays, there is a significant velocity gradient in both the radial and axial directions.[1, 2] These gradients vary according to the design of gas nozzles and the relative positioning between gas jets and the stream of metal (e.g. in atomization) or slurry (e.g. in flash smelting). Thus, atomization results in a wide droplet distribution and each droplet in that distribution finds itself in a different local gas condition of velocity, temperature and chemistry (for reaction systems). Subsequent evolution of droplet chemistry and/or microstructure depends on this initial condition and on how it couples and moves with the evolving gas characteristics in the spray. Thus, using gas generated sprays, it is very complex to identify how individual process variables contribute and control each of these coupled phenomena or resulting parameters for individual droplets or the mass of droplets in the spray. While many mathematical models have been developed of sprays and they attempt to simulate coupled droplet transport, they do not provide insight into the relative contributions of different mechanisms of transport. This is primarily because the basic fundamental heat transport between droplet and gas cannot be isolated from other gas spray phenomena experimentally such as two-way thermal coupling [3]. Thus, unambiguous experimental validation of heat transfer of large and complex industrial spray models is still not feasible. Hence, the validity of spray models remains in question and the approach required to optimize spray processes cannot be clearly identified despite numerous efforts to model these spray systems.

Recently, the development of single fluid atomization systems [4] for high temperature melts has enabled the experimental validation of droplet cooling models [5]. Since, in single fluid atomization (e.g. Impulse Atomization—IAP) stream break-up is achieved by mechanical means, the role and presence of the gas is primarily important for heat extraction. It is feasible in these systems to utilize the gas primarily for heat transfer to and from droplets.

The work of Wiskel et al. [5] has presented experimental validation of droplet cooling using IAP [4]. The model they proposed and validated is a thermal model. Chemical segregation within the alloy droplet is not taken into account. A second model incorporates this chemical segregation (microsegregation) within the droplets [6], while simulating the thermal profile of a cooling droplet. This second model uses the modified heat transfer coefficient (described in the next section) validated and used in the original thermal model. These two models will be used here to explore the effect of process variables such as droplet size, type of gas, droplet-gas relative velocity and gas temperature on heat transfer from the droplet. AA 6061 will be used as the melt material. The results and droplet transport will finally be analyzed with respect to presenting a unified theory for droplet-gas transport.

Model

Since two separate model results are presented, each model is briefly introduced. The thermal model is described first followed by the microsegregation model.

Thermal model

In a single fluid atomization system, droplets are formed on exit from an orifice with a known initial velocity [7]. Subsequent trajectory of the droplet depends on the value of this initial velocity, on gravity and on drag. The net force (instantaneous acceleration) on the droplet can be written as:

$$\frac{\mathrm{d}v}{\mathrm{d}t} = \frac{\rho_\mathrm{p} - \rho_\mathrm{f}}{\rho_\mathrm{p}} g - 0.75 \frac{\rho_\mathrm{f}}{\rho_\mathrm{p}} \frac{C_\mathrm{d}}{D_\mathrm{p}} v^2 \tag{1}$$

where v is the relative velocity between the droplet and the atomization fluid ($v_\mathrm{gas} = 0$); ρ_p and ρ_f are the densities of the droplet and atomization gas, respectively; C_d is the drag coefficient; and D_p is the droplet diameter. C_d is calculated from (Yule 1994):

$$C_\mathrm{d} = \frac{18.5}{Re^{0.6}} \tag{2}$$

and

$$Re = \frac{v D_\mathrm{p} \rho_\mathrm{f}}{\mu_\mathrm{f}}. \tag{3}$$

The models used in this work simulate the trajectory and heat transport of a single droplet unaffected by others in the

spray with a set initial velocity and temperature. Accounting for droplet interactions in a spray can be accommodated by incorporating the effect of near neighbors on drag in the flow and coupled heat transfer [8]. The work presented here will focus on the exchange of heat transfer between a single droplet and its surrounding gas. The basis for such a model and its validation has been presented in detail elsewhere and the reader is referred to the work of Wiskel et al. [5, 9] for the detailed description of the model formulation and validation. Elements of the thermal model will be briefly given here. The droplet temperature calculated using the lumped capacitance model is given by:

$$\frac{dT_m}{dt} = -\frac{h_{total}A}{\rho V C p_m}(T_m - T_\infty) \quad (4)$$

where T_m is the droplet temperature during solidification, t is time, h_{total} is the total heat transfer coefficient, ρ is the droplet density, A and V are the surface area and the volume of the droplet, respectively, Cp_m is the integral heat capacity and is given in Eq. 4 which accounts for the solidification enthalpy, T_∞ is the gas temperature in the free stream. Cp_m is given by:

$$Cp_m = \frac{dH}{dT_m} = -\frac{df_s}{dT_m} \cdot \Delta\text{Latent} + Cp \quad (5)$$

where H is the droplet enthalpy, f_s is the fraction solid, ΔLatent is the solidification enthalpy, and Cp is the heat capacity of the droplet. In general f_s and ΔLatent can represent any source term other than solidification such as a chemical reaction. The total heat transfer coefficient is given by both the convective and radiative components. We assume that the convective term is dominant.

In this model, the use of modified Whitaker correlation was proposed to account for the heating of the gas at the droplet boundary layer. In addition, it was shown that in calculating the droplet heat transfer coefficient using the Nusselt number, the thermal conductivity of the gas must be evaluated at the droplet surface temperature. For droplets less than 1 mm, this is considered to be nearly the same as the bulk temperature of the droplet as the droplet Biot number is usually $\ll 0.1$.

Temperature dependent thermophysical properties of AA6061 and of the gases are given in Wiskel et al. [5]. The rate of heat extraction in the present work is assessed by calculating the cooling rate of a solidifying AA6061 droplet. This model can be used with a zero or non-zero primary phase nucleation undercooling (user defined). For the case of zero undercooling, the cooling rate in this paper is defined as $(T_{liq} - T_{sol})/t_f$. The subscripts 'liq' and 'sol' represents the liquidus and solidus temperature of the alloy, respectively, and t_f represents the solidification time. This definition of cooling rate will henceforth be called 'Definition I' of cooling rate. In the case when the primary phase undercooling is non-zero, the cooling rate is defined as $(T_{nuc} - T_{sol})/t_f$. Here, $T_{nuc} = T_{liq} - T_u$ where T_u is the degree of undercooling. This definition of cooling rate will henceforth be called the 'Definition II' of cooling rate. The initial droplet temperature in all the simulations was 1000 K.

Microsegregation model

The microsegregation model has been developed and validated for the Al-Cu system [6, 10]. This model uses the Rappaz–Thevoz microsegregation model [11] for a single equiaxed grain growing like a spherical envelope in an undercooled droplet. This spherical grain contains the dendritic solid with interdendritic liquid and the solute mass transport (microsegregation) takes place between the solid and the liquid. The model takes into account the rate of growth of the solid–liquid interface using LKT dendrite kinetics [12]. As the envelope covers the entire droplet, the remaining liquid solidifies according to Scheil condition and subsequently, eutectic solidification completes the solidification. The Scheil type of solidification follows the thermal solidification model closely. Hence, the primary difference between this model and the thermal model is in the use of dendrite kinetics in the early stages of solidification when the envelope growth is simulated. This model uses the same gas-to-droplet heat transfer mechanism as the thermal model by using the modified Whitaker correlation. The initial values for this model are the same as for the thermal model, viz., melt temperature, droplet velocity, and material and gas properties. In addition, the model also requires user-defined nucleation undercooling temperature as well as nucleation position. Based on previous modeling work on Al–Cu system [6], the nucleation undercooling of 20 K was used in all simulations and a nucleation position exactly between droplet center and periphery ($0.5R$, where R is the droplet radius) was chosen.

The AA6061 alloy has a nominal composition [13] of—Si (0.4–0.8), Mg (0.8–1.2), Fe (0.7 max), Cu (0.15–0.4), and Al (balance). Since this model was developed for a binary alloy system, the AA6061 system has to be approximated as a binary system, which is made up of Al and one of the alloying elements. The freezing range of AA6061 is between 924.6 K and 855 K [5]. If one considers the freezing range of Al–Si, Al–Mg, Al–Fe, and Al–Cu systems, eutectic of Al–Mg is 724 K (too low in comparison with AA6061), Al–Fe is 928 K (too high in comparison with AA6061), and that of Al–Cu is 821 K (again much lower than AA6061). On the other hand, Al–Si system has a eutectic at 850 K. Since this value is closest to the actual AA6061 alloy, for modeling purposes, it is reasonable to approximate AA6061 as an Al–Si

Table 1 Values of phase diagram parameters used in the model

Phase diagram parameter	Value
Melt (initial liquid) composition, C_0	1.431% Si
Initial solid composition	0.187% Si
Liquid composition at eutectic temperature	12.6% Si
Solid composition at eutectic temperature	1.65% Si
Liquidus temperature, T_l	924.6 K
Eutectic temperature, T_e	855 K
Liquidus slope, m_l	−6.23
Partition coefficient, k	0.131

system. The Al–Si approximation was based on a linear phase diagram (straight line approximation of liquidus and solidus) with eutectic at 855 K. The validated model for Al–Cu system [6] uses a similar linear approximation for the Al–Cu phase diagram. The Si content for the melt composition was chosen based on the liquidus of AA6061 of 924.6 K. Table 1 gives the values of the phase diagram values used in this model.

Figure 1a shows a typical thermal plot from the microsegregation model. Figure 1b shows the solute concentration in the solid phase as a function of fraction solid. The legends in the two figures are the same. Line A is the alloy liquidus and point B is the nucleation temperature (with 20 K undercooling). Points BC represents the initial growth of the dendrites, which grows immediately after nucleation,

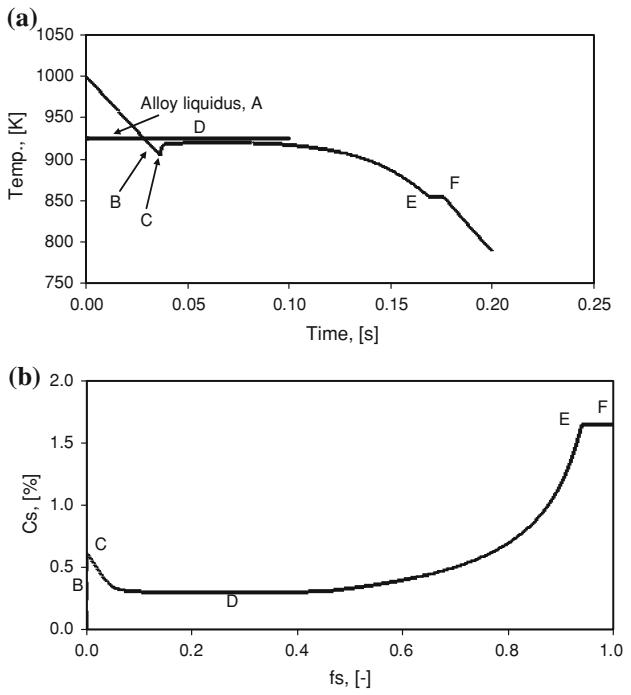

Fig. 1 Simulation result from the microsegregation model for AA6061, 350 μm droplet in N_2, (**a**) thermal plot, and (**b**) solute concentration as a function of fraction solid

and CD represents recalescence, when the latent heat generated is greater than the convective heat loss. DE is the Scheil type of solidification and EF is the eutectic solidification. Since a primary phase nucleation undercooling is always used in this model, the cooling rate for this model is always the Definition II of cooling rate. In this case it is the time taken for the droplet to cool from the nucleation temperature (which is less than the equilibrium value due to undercooling) to the eutectic temperature.

The solid phase solute profile (see Fig. 1b) clearly shows the change in chemical composition in the solid phase as a result of the microsegregation. For example, in Fig. 1b, the solute content in the solid increases during the initial growth of dendrite (points BC) and decreases during recalescence (points CD).

Results

Some preliminary cooling rate results are presented first. Table 2 shows the cooling rate results for two droplet sizes (350 μm and 50 μm) atomized under two gases (He and N_2) at two different gas temperatures (T_{gas} = 300 K and 800 K) with 0.5 m/s initial velocity. The cooling rates are calculated under the following scenarios: thermal model—0 K and 20 K primary nucleation undercooling and microsegregation model—20 K undercooling. Column IV of the table shows the cooling rate from thermal model under 0 K undercooling calculated using Definition I. Column V shows the cooling rate with Definition I but 20 K undercooling and column VI shows the cooling rate with Definition II with 20 K undercooling. The cooling rate with Definition II from microsegregation model is shown in column VII. Results from columns IV and V thus compare the cooling rate results with and without the primary phase undercooling. This comparison is done in column VIII by calculating the percentage difference in cooling rates in columns IV and V. Similarly, results from columns VI and VII are compared in column IX by calculating the percentage difference in cooling rates between thermal and microsegregation model when the same undercooling and same definition of cooling rates are used. Thus, the effect of undercooling as well as the model type on cooling rate is estimated.

In the presence of undercooling, the cooling rate differs by 3–4% (column VIII). When different models are compared (column IX) the difference in cooling rates are in the same range, even smaller in some cases. Note that these results are for a very wide range of cooling rates (10^1–10^4 K/s). Thus, it can be clearly seen that (1) presence of undercooling does not effect the cooling rate significantly, and (2) use of thermal or microsegregation model also does not make a significant difference in the cooling rate

Table 2 Cooling rate results from thermal and microsegregation models

Gas	T_{gas} (K)	Drop. size (μm)	Cooling Rate (K/s)				% Diff in Cooling Rate	
			Thermal model			Microseg. model	Columns IV–V	Columns VI–VII
			0 K, Def.I	20 K, Def.I	20 K, Def.II	20 K, Def.II		
N_2	800	350	59.3	61.2	43.6	42	3.2	3.7
		50	1834	1885.7	1349.5	1298.9	2.8	3.7
	300	350	367.9	383.9	274.2	277.1	4.3	1.1
		50	9504.3	9844.4	7054.7	6726.1	3.6	4.7
He	800	350	225.8	233.2	166.4	164.6	3.3	1.1
		50	9447.5	9765.7	6957.3	6877.4	3.4	1.1
	300	350	1141.6	1187.5	847.4	871.4	4.0	2.8
		50	45194.8	49396.8	33293.2	33478.2	9.3	0.6

Table 3 Ratio of cooling rates for different conditions obtained from the thermal and the microsegregation model

Gas temp. (K)	Ratio of cooling rate between thermal and microsegregation model			
	0.5 m/s		30 m/s	
	He	N_2	He	N_2
300	1.31	1.33	1.31	1.33
800	1.37	1.41	1.38	1.45

analysis. Based on this result, the subsequent cooling rate analysis is carried out by comparing the cooling rate results from thermal model with 0 K undercooling with Definition I of cooling rate and microsegregation model with 20 K undercooling with Definition II of cooling rate. The cooling rates obtained from these two models under different cooling rate definitions are analyzed further.

Table 3 shows the ratio of calculated cooling rates between thermal and microsegregation model obtained from these two models (with appropriate cooling rate definition and undercooling). The result is shown for 0.5 m/s and 30 m/s initial velocity under He and N_2 gases at 300 K and 800 K, respectively. The thermal model consistently gives a higher cooling rate for all cases. This ratio is between 1.3 and 1.4 as the gas temperature increases from 300 to 800 K. This is true for both gas types and for either initial droplet velocities. Figure 2 shows this ratio of cooling rates between thermal and microsegregation model as a function of particle size (50 and 350 μm) for He and N_2 gas at 300 and 800 K gas temperature.

Consider Table 4, which shows the solidification time, t_f, for a 350 μm droplet cooled under He gas at 300 K and 800 K for two different initial droplet velocities. As can be seen from the table the solidification times from the microsegregation model is marginally smaller than those from the thermal model. The heat generation term is

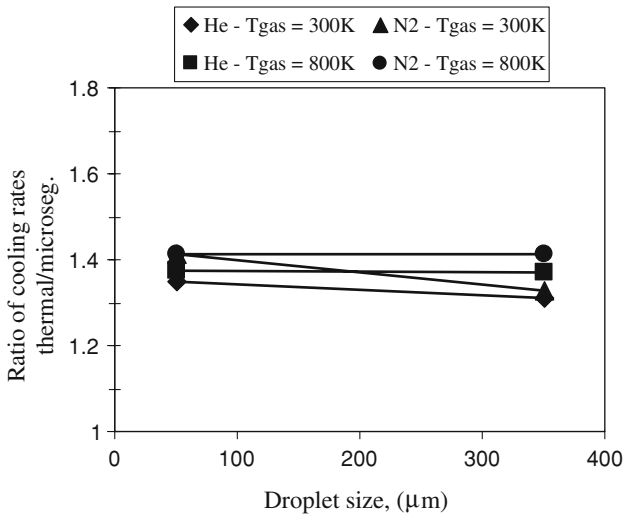

Fig. 2 Ratio of cooling rates between thermal and microsegregation models as a function of droplet size, gas type, and gas temperature

Table 4 Solidification times for a 350 μm droplet under He gas from thermal and microsegregation model for two different gas temperatures and two initial droplet velocities

Gas temp. (K)	0.5 m/s		30 m/s	
	Thermal (s)	Microsegregation (s)	Thermal (s)	Microsegregation (s)
300	0.060	0.057	0.025	0.024
800	0.308	0.301	0.222	0.219

different between the two models since the dendrite kinetic governs the latent heat release for some part in the microsegregation model. The microsegregation model indicates that the dendrite velocities can reach up to 1.8 cm/s (350 μm droplet in He at 300 K) at the onset of recalescence. Of course, the onset of recalescence reduces this rate down to 0.6 cm/s. The effect of the fast growth rate is to

lower the solidification time, but the presence of recalescence and eutectic (isothermal) cooling tends to lengthen the total solidification time. Following this interplay between different regimes of solidification, as seen during the simulation of microsegregation, it is not surprising to see that the total solidification time from the thermal and microsegregation models is very close to each other.

The cooling rate from microsegregation model is lower because the presence of 20 K of primary undercooling reduces the freezing range. Hence according to the definition of cooling rate (Definition II), the cooling rate from microsegregation is consistently lower even when the solidification time is almost the same from the two models. The freezing range of the alloy is approximately 70 K and when one considers a 20 K undercooling, the freezing range reduces by $\sim$30% for Definition II (microsegregation model) as compared to Definition I (thermal model). This explains the 1.3–1.4 ratio between the thermal and the microsegregation models. In summary, the presence of undercooling or the use of thermal or microsegregation model does not affect the cooling rate analysis. The parameters that affect the cooling rates in a solidifying droplet are evaluated next.

Effect of different variables

It is important to note that in all cases reported in this paper, the velocity of droplets never reaches the terminal velocity before the droplet temperature falls below the eutectic temperature. Thus, throughout the solidification period there is always a changing relative velocity between droplet and gas. The cooling rate results are described in terms of effect of four variables, namely, initial droplet velocity, droplet size, gas type, and gas temperature. The model results for droplet cooling rate from the thermal model are presented in Figs. 3–5 and 8. The corresponding results for droplet cooling rate from the microsegregation model are presented in Figs. 6, 7 and 9.

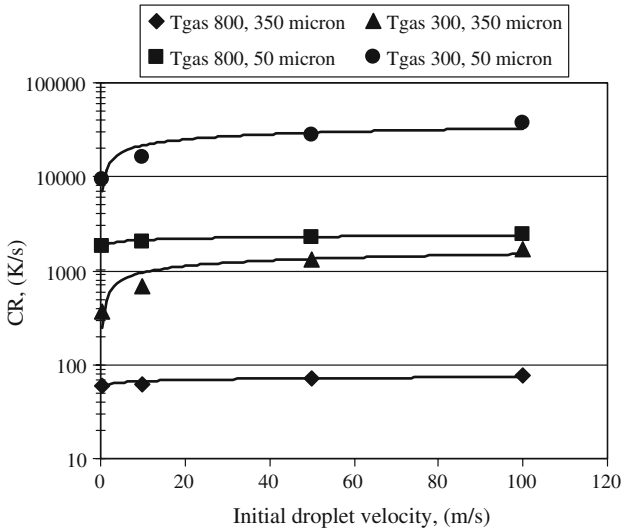

Fig. 3 Thermal model results showing the effect of initial droplet velocity and gas temperature for the cooling of AA6061 droplets having 350 and 50 μm diameters in nitrogen gas

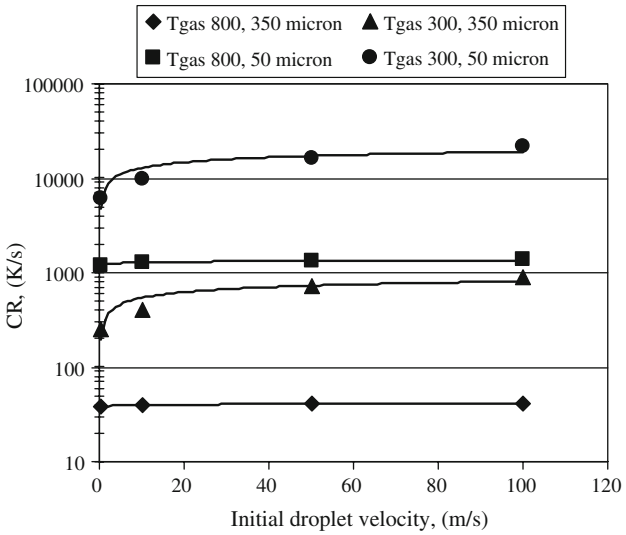

Fig. 4 Thermal model results showing the effect of initial droplet velocity and gas temperature for the cooling of AA6061 droplets having 350 and 50 μm diameters in argon gas

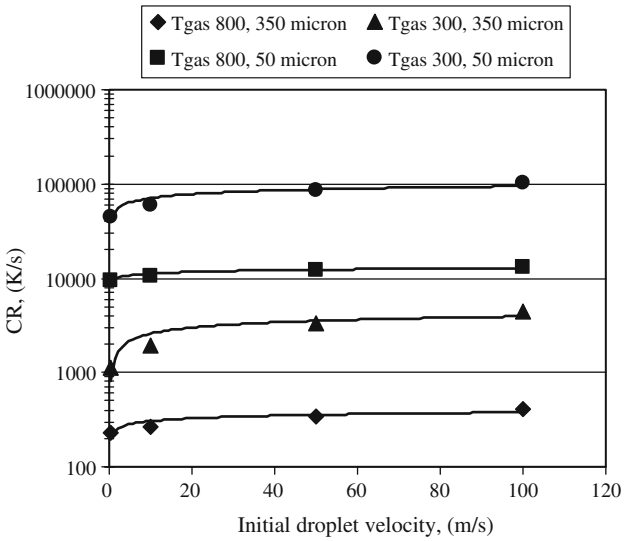

Fig. 5 Thermal model results showing the effect of initial droplet velocity and gas temperature for the cooling of AA6061 droplets having 350 and 50 μm diameters in helium gas

Effect of droplet initial velocity

The effect of initial droplet velocity from the thermal model are presented for 350 and 50 μm droplets in Figs. 3–5 for heat transfer in nitrogen, argon, and helium,

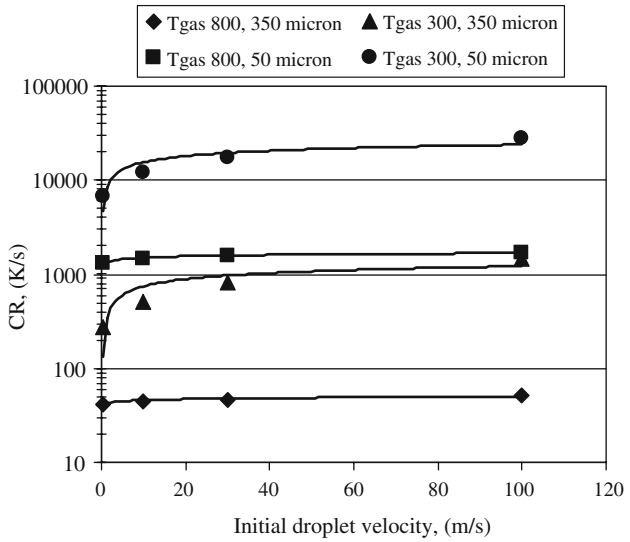

Fig. 6 Simulation results for cooling rate under nitrogen gas as a function of initial velocity of droplet for two droplet sizes from the microsegregation model

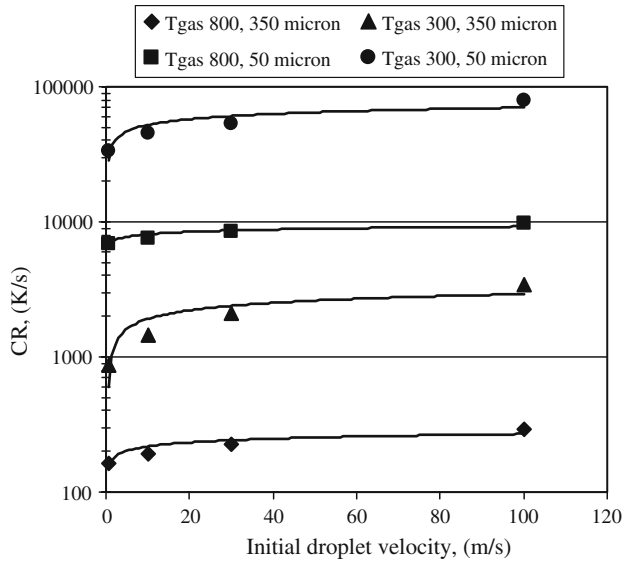

Fig. 7 Simulation results for cooling rate under helium gas as a function of initial velocity of droplet for two droplet sizes from the microsegregation model

respectively. From Fig. 3, it is evident that for a 350 and a 50 μm droplet, the largest effect of initial droplet velocity occurs up to about 30 m/s when the gas temperature is 300 K. Higher initial velocities have a negligible impact on increasing the heat extraction from the droplets (i.e. increasing droplet cooling rate). When the gas temperature is at 800 K, the effect of initial velocity is negligible for both droplet sizes. This is clear from the fact that the driving force for heat transfer is greatly reduced. However, the cooling rate for 350 and 50 μm droplets are different by at least one order of magnitude regardless of the initial velocity of the droplet or the gas temperature. This seems to indicate that the surface-to-volume relationship for the droplets is a primary variable in transport between the droplet and the gas. In other words, a sevenfold reduction in droplet size has a greater impact on heat transfer compared to a 100-fold increase in initial droplet velocity.

Results from the microsegregation model for the effect of initial droplet velocity under nitrogen and helium gas are shown in Figs. 6 and 7, respectively. Figure 6 shows the cooling rate of 350 and 50 μm droplet under nitrogen gas for two different gas temperatures. The same range of initial velocities is used as for the thermal model. The predictions clearly show that for 800 K of gas temperature, there is negligible change in cooling rate with a 100-fold increase in droplet initial velocity. On the other hand, irrespective of the initial droplet velocity, a decrease in droplet size from 350 to 50 μm results in a significant increase in cooling rate (~40 times). This also, is true for both gas temperatures. Figures 4 and 5 show the same results for argon and helium gases, respectively, from the thermal model. Likewise, the microsegregation model result for helium gas, shown in Fig. 7 shows similar trends. Thus, with respect to the effect of initial droplet velocity on the droplet cooling rate, same trends are obtained from both models.

Effect of droplet size

The effect of droplet size on droplet cooling rate can also be seen from Figs. 3–7. The figures show that as the droplet size decreases, the cooling rate increases. Irrespective of the initial droplet velocity, gas type, or the gas temperature, the smaller droplet size results in consistently higher cooling rates. Once again, both the thermal model as well as the microsegregation model show the same results.

Effect of gas temperature

A comparison of the cooling rate of 350 and 50 μm droplets as a function of gas temperature from thermal model is shown in Fig. 8. The gas temperature has a more important effect on the rate of heat transferred than the initial droplet velocity. When the initial temperature difference between gas and droplet is reduced from 700 to 300 K, the cooling rate is decreased by an order of magnitude for both 350 and 50 μm droplets. As the gas temperature increases, the cooling rate decreases. This is due to the reduced driving force for heat transfer to the gas. Despite the reduction in cooling rate with increased gas temperature, the 50 μm droplet experiences a cooling rate which is at least one order of magnitude higher than that for the 350 μm droplet.

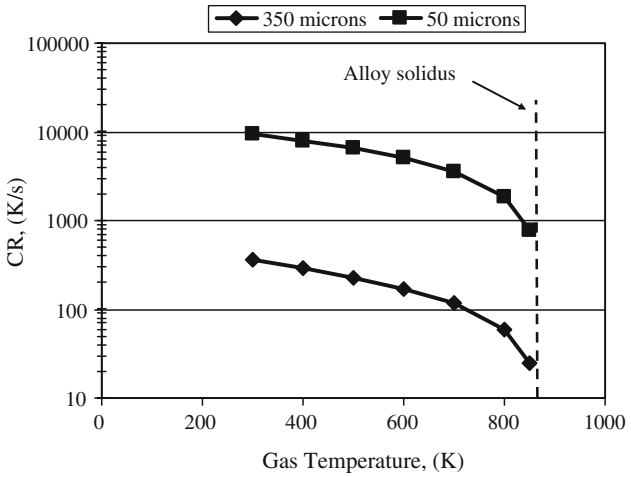

Fig. 8 Cooling rate of AA6061 droplets from the thermal model in nitrogen for 350 and 50 μm as a function of gas temperature with an initial droplet velocity of 0.5 m/s

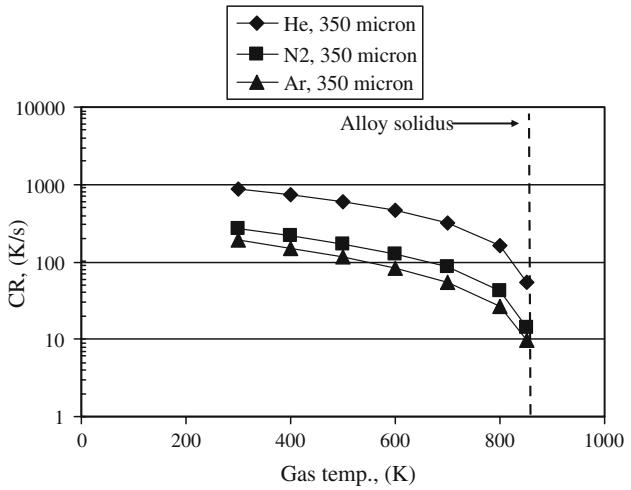

Fig. 9 Simulation results for cooling rates as a function of gas temperature for three different gases. Results obtained from the microsegregation model

The decrease in cooling rate with increased gas temperature is also observed in the comparison with the microsegregation model (Fig. 9). Cooling rates for a 350 μm droplet is plotted as a function of gas temperature for helium, nitrogen, and argon gases. The initial droplet velocity was the same (0.5 m/s) in all cases. As the gas temperature is increased from 300 K to 800 K, the cooling rate decreases by an order of magnitude. This is true for all gas types. Furthermore, this is the same trend as obtained from the thermal model.

Effect of gas type

The cooling rates are slightly higher for the droplets solidifying in nitrogen than in argon (see Figs. 3, 4). The droplet size is again the dominant variable in heat transfer as shown in these two figures, and gas temperature has a more marked impact on cooling rate than initial velocity.

The cooling rate for droplets solidifying in helium is shown in Fig. 5. Even though helium is considerably lighter than nitrogen and argon, the effect of initial velocity on cooling rate is even smaller than is observed in Figs. 3 and 4 for nitrogen and argon, respectively. Also evident, is that the cooling rate of droplet solidification is always an order of magnitude higher in helium than in nitrogen and argon. This is primarily due to the thermal conductivity of helium being one order of magnitude higher than that for nitrogen or argon.

Figure 9 shows the effect of gas type on the cooling rates from the microsegregation model for three different gases. There is a marked decrease in cooling rate as the gas temperature is increased (2–3 times depending upon the gas type). Furthermore, the cooling rate for a droplet solidifying under helium is higher than that in argon or nitrogen. This is because of the higher conductivity of the helium gas compared to the other two gases as explained before.

In summary, while there is effect of droplet size and gas temperature on the cooling rate of solidifying droplets, the change in initial velocity of the droplet hardly plays any role in affecting the droplet cooling rates. Thus the critical variables that govern the droplet cooling rates are the droplet size, gas type, and the gas temperature. This conclusion is based on the results obtained from thermal as well as microsegregation model. In other words, microsegregation within the droplet does not change or affect the critical variables that govern the droplet cooling rate. This is not surprising since the variables, droplet size, gas type, and gas temperature, are independent of the mass transport happening within the droplet. Thus, the cooling rate trends as a function of gas temperature, droplet size, droplet initial velocity, and gas type are the same for the two models. For the dominant effect of gas temperature and droplet size on droplet cooling rate is further discussed in the section "Discussion."

From the above, it is apparent that for a given gas type, both gas temperature and droplet size are the two important variables in droplet-gas heat transfer. Figure 10 shows the effects of these process variables for the 350 μm droplet in particular. The results are from the thermal model. The filled squares are the cooling rate versus gas temperature results from Fig. 8, replotted in Fig. 10. Note that if the gas temperature increases by almost a factor of three (300–850 K) the cooling rate correspondingly decreases by a factor of almost 17 (425–25 K/s). Associated with those results is the distance that the droplets have traveled when they have fully solidified. For a gas temperature of 300 K, a cooling rate of about 425 K/s is achieved and the droplet is fully solidified by the time it reaches several centimeters below its point of initiation. Note that as the gas temperature increases, the distance traveled to reach complete

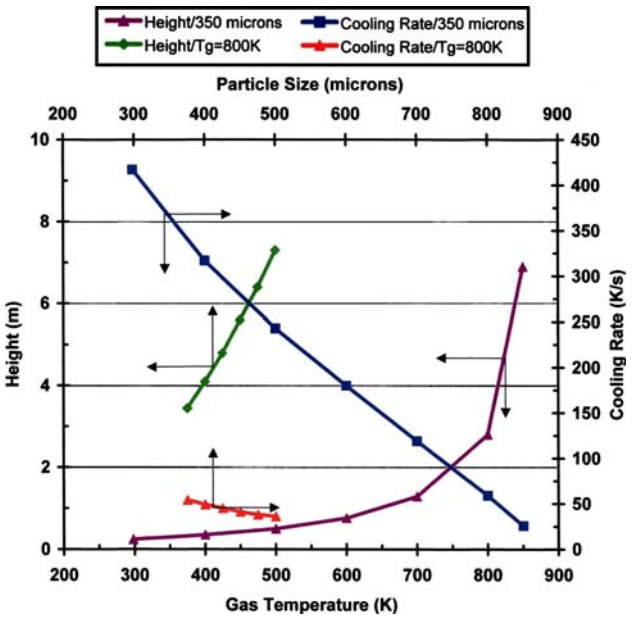

Fig. 10 Summary of a AA6061—350 μm droplet cooling in nitrogen

solidification increases dramatically. When T_{gas} is 850 K, the droplet is fully solidified at 7 m. This is consistent with the fact that the driving force for heat transfer is reduced as the gas temperature is increased.

For a fixed high gas temperature of 800 K, the effect of droplet size is also shown in Fig. 10. The filled triangles clearly show that as the particle size is increased from 350 to 500 μm, the cooling rate is halved. Note that from Fig. 8, for a 50 μm droplet and a gas temperature of 800 K, the cooling rate is about 800 K/s. Thus the effect of droplet size becomes more important as its diameter decreases, consistent with earlier predictions indicating that the surface-to-volume ratio of the droplets is a critical variable.

Discussion

The droplet temperature calculated using the lumped capacitance model is given by Eqs. 4 and 5 given above. The total heat transfer coefficient is given by both the convective and radiative components. Assuming that the convective component is dominant and is calculated using the modified Whitaker correlation given by Eq. 6:

$$Nu = \frac{h_{conv}D}{k_s} = 2 \cdot \frac{B}{k_s \cdot (m+1)} \cdot \frac{(T_m^{m+1} - T_\infty^{m+1})}{(T_m - T_\infty)} + (0.4Re^{0.5} + 0.06Re^{0.67})Pr^{0.4}\left(\frac{\mu_{bulk}}{\mu_{surf}}\right)^{0.25} \quad (6)$$

where k_s is the gas thermal conductivity evaluated at the droplet surface, superscripts m and $(m + 1)$ are indices for the numerical calculation, Re and Pr are the droplet Reynolds and Prandltl numbers, respectively, and μ_{bulk} and μ_{surf} are the gas viscosities at the temperature of the free flow gas and of the droplet, respectively. Simplifying the modified Whitaker correlation for purposes of this derivation yields:

$$Nu = \frac{h_{conv}D}{k_s} = 2.0 + (0.4Re^{0.5} + 0.06Re^{0.67})Pr^{0.4}\left(\frac{\mu_{bulk}}{\mu_{surf}}\right)^{0.25}. \quad (7)$$

For a spherical droplet, the non-dimensional form of Eq. 4 with the substitution of Eq. 4 for h_{conv} yields the following dimensionless equation:

$$\frac{d\theta}{d\tau} = -\frac{k_s t^*}{D^2 \rho Cp_m}(\theta - 1)\left(2.0 + (0.4Re^{0.5} + 0.06Re^{0.67})Pr^{0.4}\left(\frac{\mu_{bulk}}{\mu_{surf}}\right)^{0.25}\right) \quad (8)$$

where θ is T/T_∞ and τ is t/t^*. t^* is a reference time (e.g. the solidification time of the droplet).

From Eq. 8 the dimensionless terms governing gas-droplet heat transfer are θ, Re, Pr, $\frac{k_s t^*}{D^2 \rho\ Cp_m}$, and $(\frac{\mu_{bulk}}{\mu_{surf}})$. The effect of Re, Pr, and $(\frac{\mu_{bulk}}{\mu_{surf}})$ on the dimensionless droplet cooling rate is dampened by the fractional power on each of these terms. Thus, it is not surprising that in the calculations shown earlier, droplet-gas relative velocity had minimal effect on droplet cooling rate. On the other hand, θ and $\frac{k_s t^*}{D^2 \rho\ Cp_m}$ have a more important effect on droplet cooling rate. θ is essentially the driving force between gas and droplet for heat transfer. A closer look at the second term yields:

$$Fo^* = \frac{k_s t^*}{D^2 \rho\ Cp_m} \quad (9)$$

where Fo^* is a modified Fourier number for droplet-gas thermal transport. It relates the ability of the gas to absorb the heat dissipated by the droplet, by solidification in this case or by reaction in the general case. Note that from Eq. 9 the thermal conductivity of the gas at droplet temperature is an important variable. Thus, the more conductive the gas at higher temperatures, the faster the heat transport can be carried out. Conversely, the larger the amount of heat to be dissipated by the droplet (Cp_m), the more time will be required to complete the transport in order to maintain the same Fo^* value. Equally interesting is the square relationship on droplet diameter in the denominator of Equation (9) which reflects the fundamental importance of the droplet surface area in thermal transport. Clearly this supports the effect of droplet size presented earlier in this work and emphasizes that the smaller the droplet the faster the transport. Hence, for a

given gas type, gas temperature and droplet size (i.e. droplet surface area) are the two most important variables in droplet thermal transport. In dimensionless terms, Fo^* and θ are the primary variables affecting droplet-gas transport.

This analysis, however, is not complete. It has been shown in a few studies that for the same alloy the same droplet size atomized in different atomizing processes can have different microstructures [3, 14]. A few examples are discussed here.

Figures 11 and 12 show the microstructure and cell spacing versus particle size for spherical bronze, respectively. All the particles in Fig. 11 are of the average sieve size of 328 μm. The droplet in Fig. 11a was atomized using the horizontal gas atomization process, while IAP was used to generate the particles shown in Fig. 11b and c. The very different range of microstructures clearly illustrate that for the same size of droplet and same alloy, different microstructure can be achieved from different processes or from the same process using different operating conditions. In this case, IAP powders yielded the same microstructure as horizontal gas atomized powder by reducing the atomized melt temperature. This would have the effect of reducing the gas thermal conductivity which in gas, increases with temperature. Thus a lower melt temperature will yield a lower gas thermal conductivity, thus reducing the rate of heat loss from the droplet to the gas. This is evident when comparing Fig. 11b and c. Figure 12 shows the cell spacing versus particle size relationship for a wide range of particle sizes. The effects illustrated in Fig. 10 are clearly evident over a range of sizes.

Figure 13 shows a comparison for Al–Fe–Ni alloy. Here the powder microstructure generated from three atomization processes are compared: Alcoa gas atomization, centrifugal atomization, and IAP [7, 14]. A comparison of the first two processes could lead to the conclusion that particle microstructure is independent of atomization process. However, the results from IAP powder clearly show that this is not to be the case.

Another comparison was presented by v. Freyberg et al. [3] for Cu–6Sn powders . Here again, the same size powder particle reveals a different microstructure when atomized with the same gas but using different processes. This trend was observed over a range of particle sizes [3] and was shown to be attributed to the phenomenon of two-way thermal coupling in the spray.

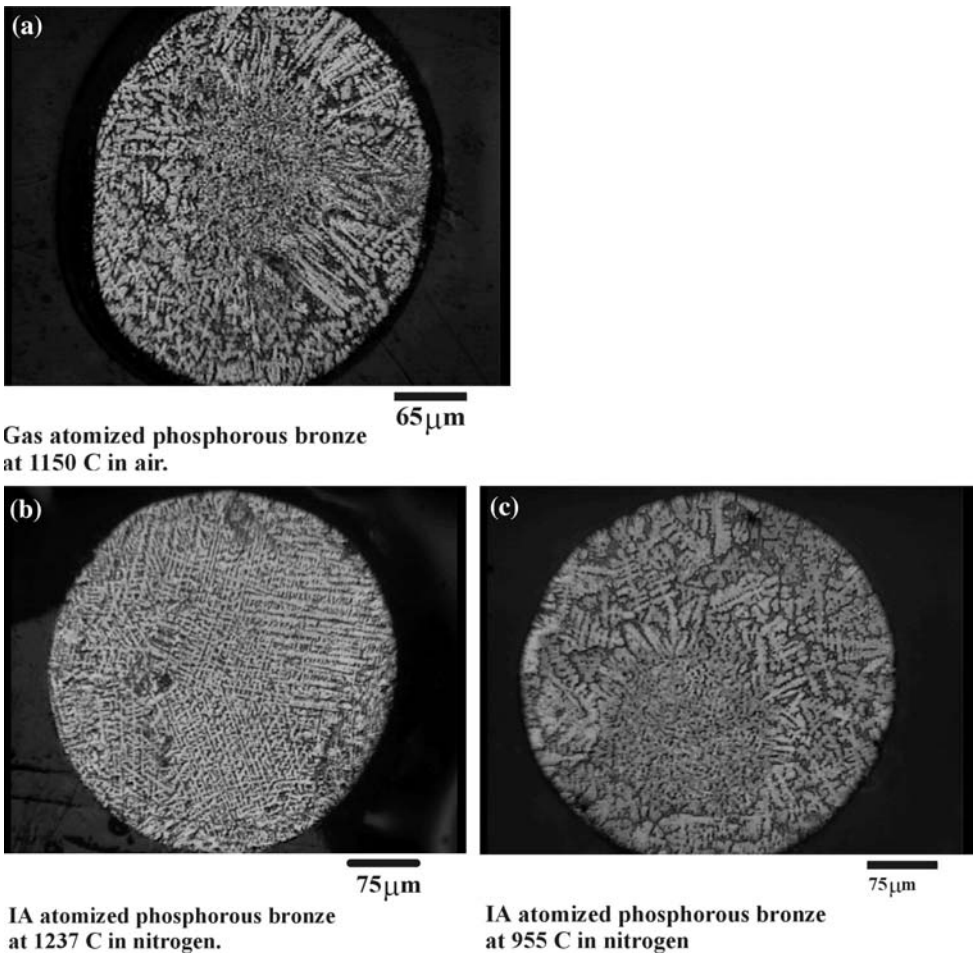

Fig. 11 Microstructures of 328 μm phosphorous bronze powder atomized under different operating conditions in different atomization processes

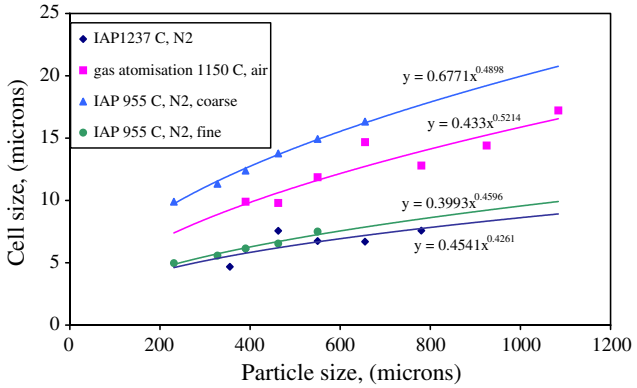

Fig. 12 Cell size versus particle size for phosphorous bronze powders from different atomization processes. The coarse and fine structures referred to here correspond to the microstructure evident in coarse and fine structures shown in Fig. 11b and c

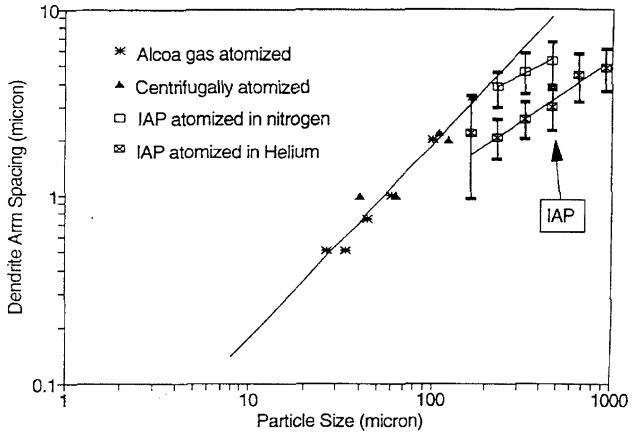

Fig. 13 Al–3.7Ni–1.5Fe (wt%) alloy microstructure measurements compared for different gas atomization processes [4]

If we consider melt spray generated by a gas, it has been shown that the duration of a large relative velocity between droplets and gas is very small relative to the total trajectory of the droplet [3]. As the droplet travels in its trajectory in the spray, it will exchange heat with the adjacent gas. If the relative motion between droplet and gas remain small, the gas temperature adjacent to the droplet will increase, reducing the driving force for further droplet cooling. This phenomenon is called two-way thermal coupling. It has been shown that by evaluating the thermal Stokes number [3, 8], the extent of two-way thermal coupling may be evaluated.

Work by v. Freyberg et al. [3] has shown that when an atomization process has a propensity for two-way thermal coupling, the resulting droplet microstructure is coarser than the corresponding droplet size generated under process conditions with low two-way thermal coupling. It was shown that the exit gas temperature in a spray chamber is related to the thermal Stokes number. The lower the thermal Stokes number, the higher the amount of two-way thermal coupling and the higher the gas temperature. The overall exit gas temperature in a spray chamber can therefore be used as a measure of the two-way thermal coupling in a system. Thus, the thermal Stokes number should be included with θ and Fo^* to fully assess the thermal exchange between droplet and gas. Hence, it can be stated that when the evolution of the dimensionless gas temperature and the Fo^* are similar between two sprays, droplet transport will also be similar. Thus, if identical sized droplets in two different sprays have identical cooling history, they will result in identical microstructure.

Conclusions

It is clear from the results presented in this work that calculated cooling rates of droplets are virtually independent of the type of model used for the calculation. Both the thermal and the microsegregation models yield nearly similar cooling rates when the temperature range for solidification is the same.

It has been shown in this work that droplet diameter and gas temperature are the two most important variables in transport between droplets and gas. These critical parameters are not affected by the microsegregation within the droplet. For the larger particles (>200 μm) the temperature driving force between gas and droplet temperature is the most critical variable. For droplets <200 μm the droplet diameter becomes a significant variable. In all circumstances the droplet initial velocity is not a significant parameter in heat transfer from the droplet. This is supported by the fact that in the cooling models the droplet relative velocity is used to calculate the Nusselt through the modified Whitaker correlation. In this correlation, the velocity appears in the Re number to the 1/3 power. Thus the effect of droplet velocity is reduced in effect compared to the temperature driving force between gas and droplet or the droplet diameter. Finally, helium provides the highest rates of heat transport compared to nitrogen and argon due to its higher thermal conductivity. The effect of droplet relative velocity with the gas is important as far as it affects the degree of two-way thermal coupling between droplet and gas. Similarity of reaction rates or powder microstructure will be achieved when the thermal stokes number, Fo^* and θ are similar between two sprays.

Acknowledgements The author wishes to acknowledge funding for this work from the Natural Science and Engineering Research Council of Canada (NSERC) and from the Canada Council for the Arts for award of a Killam Research Fellowship. The contribution of Karine Navell in making the cell spacing measurements presented in Fig. 12 are also acknowledged.

References

1. Ziesenis J, Tillwick J, Krauss M, Uhlenwinkel V (2000) In: Cooper KP et al (eds) Atomization: fundamentals and practice. TMS, Warrendale, PA, pp 61–70
2. Ting J, Connor J, Ridder S (2005) Mater Sci Eng A 390(1–2):452. doi:10.1016/j.msea.2004.08.060
3. Freyberg AV, Henein H, Uhlenwinkel V (2003) Mat Trans B 34B:243. doi:10.1007/s11663-003-0011-3
4. Henein H (2002) Mat Sci Eng A 326:92
5. Wiskel JB, Henein H, Maire E (2002) Can Metall Q 41(1):97
6. Prasad A (2006) Microsegregation in rapidly solidified impulse atomized binary Al-Cu alloy. PhD thesis, University of Alberta
7. Yuan D (1997) The novel impulse atomization process. PhD thesis, University of Alberta
8. Crowe CT (2000) SDMA, University of Bremen, Bremen, Germany, pp 757–769
9. Wiskel JB, Henein H, Maire E (2002) Can Metall Q 41(2):193
10. Prasad A, Henein H, Gandin C-A (2007) In: Gandian C-A (ed) Modeling of casting, welding and advanced solidification processes XI. TMS, Warrendale
11. Rappaz M, Thevoz PH (1987) Acta Metall 35(7):1487. doi:10.1016/0001-6160(87)90094-0
12. Lipton J, Kurz W, Trivedi R (1987) Acta Metall 35(5):957. doi:10.1016/0001-6160(87)90174-X
13. Dorward RC, Bouvier C (1998) Mater Sci Eng A A254(1–2):33. doi:10.1016/S0921-5093(98)00761-8
14. Hildeman GJ, Lege DJ, Vasudevan AK (1982) In: Koczak MJ, Hildeman GJ (eds) High strength powder metallurgy aluminum alloys. TMS, Warrendale, PA, pp 249–276